IEEE Access
Multidisciplinary | Rapid Review | Open Access Journal

Received August 13, 2019, accepted September 4, 2019, date of publication September 12, 2019, date of current version September 25, 2019.

Digital Object Identifier 10.1109/ACCESS.2019.2940759

Three-Dimensional VLC Positioning System Model and Method Considering Receiver Tilt

DUCKYONG KIM[1], JONG KANG PARK[2], (Member, IEEE), AND JONG TAE KIM[1,2], (Member, IEEE)

[1]Department of Electrical and Computer Engineering, Sungkyunkwan University, Suwon 16419, South Korea
[2]School of Electronic and Electrical Engineering, Sungkyunkwan University, Suwon 16419, South Korea

Corresponding author: Jong Tae Kim (jtkim@skku.edu)

This work was supported by the Basic Science Research Program through the National Research Foundation of Korea (NRF) funded by the Ministry of Education under Grant 2015R1D1A1A01061304.

ABSTRACT In recent years, several indoor positioning systems have been extensively studied for environments where a satellite signal is typically degraded and interrupted. Among them, visible light positioning (VLP), which has several advantages such as the absence of electromagnetic interference, energy efficiency, and high bandwidth availability, has received considerable attention. However, most VLP systems are established based on two-dimensional (2D) positioning methods in which the height of the receiver is fixed or restricted and the tilt of the receiver is not considered. To solve these problems, we propose a new positioning method that can be applied to three-dimensional (3D) space. We first formulate a new mathematical model for a 3D VLC positioning system and derive the channel gain as a function of source and receiver location in Cartesian coordinates. By employing the cost function developed using the induced channel gain, we demonstrate that the proposed 3D method is more accurate compared to the 2D method in experiments. The quantitative results show an average error of 7.95 cm, in a 2.5 m $\times$ 2.5 m $\times$ 3 m region.

INDEX TERMS Visible light communication (VLC), visible light positioning (VLP), indoor positioning system (IPS), received signal strength (RSS), orthogonal code.

I. INTRODUCTION

In recent years, several studies have focused on position estimation in indoor environments, where a satellite signal is typically degraded and interrupted. Indoor positioning systems (IPSs) can be configured for various types of signals, such as infrared, ultrasound, Bluetooth, RFID, UWB, and WLAN. However, it is not easy to address the technical problems originating from short transmission distances, multipath effects, low accuracies, various signal interferences, and high design costs. To overcome these challenges, positioning systems based on visible light communication (VLC) have been studied. As visible light does not cause electromagnetic interference and has stronger anti-interference ability, it is suitable for use in RF sensitive areas, such as hospitals and airplanes [1]–[4]. Moreover, it is easy to multiplex multi-channel optical signals owing to the broad and high bandwidth availabilities [4]–[6]. The use of light emitting diodes (LEDs) as optical drivers has significant advantages, such as the energy efficiency, lower cost, longer lifetime, and cost-effectiveness for construction using the LED infrastructure already available in the environment [1], [3]–[5], [7].

Recent studies on visible light positioning (VLP) have indicated that supplementary devices, such as inertial sensors, magnetic sensors, and accelerometers, or even several extra receivers are required to improve the positioning estimation accuracy [2], [8]–[13]. Furthermore, considering the receiver tilt can improve the positioning results [14]–[18]. Some studies [14]–[16] have reported that the positioning methods that use inertial measurement unit (IMU) sensors or the ratio of the multiple received signal strength (RSS) values lead to mean errors at the centimeter scale. For image sensor-based receivers, it has been reported that the tilt can be compensated using the angle difference of arrival (ADOA) [17], [18]. Even when considering the receiver tilt, VLP systems typically use geometrical assumptions, such as fixing or limiting of the receiver height, and are performed on the 2D plane [19]–[21]. There are some studies that solved problems by applying an artificial neural network (ANN). Two of these methods [22], [23] reported high accuracy in three-dimensional space,

The associate editor coordinating the review of this manuscript and approving it for publication was Jiajie Fan.

TABLE 1. Photodiode-based VLC positioning systems.

Reference	Algorithm	Test Area	Dimension	Tilt consideration[1]	Auxiliary Device
[9]	RSS, Trilateration	5×8 m, 2×12 m,3.5×6.5 m	2D	-	Inertial sensor, Beacon
[10]	RSS, Trilateration	2.5×2.84×2.5 m	2D	-	Inertial sensor
[19]	RSS, Trilateration	0.9×0.9×0.7 m	2D	-	-
[20]	RSS, Trilateration	20×20×15 cm	2D	-	-
[21]	RSS, Trilateration	36×12×3 m	2D	-	16 LEDs
[11]	RSS, Fingerprinting	1.8×1.2×1.0 m	2D	-	4 Extra PDs
[13]	RSS, Trilateration	12×10 m ∼ 24×16 m	3D	-	Magnetic sensor, 5 Extra PDs
[24]	RSS, Optimization	1×1×1.2 m	3D	-	-
[2]	RSS, Modeling	5×4×3 m	3D	-	Accelerometer, 3 Extra PDs
[7]	RSS, AoA	2×2×1 m	3D	-	4 Extra PDs
[22]	RSS, Fingerprinting, ANN	0.9×1×0.4 m	3D	-	-
[23]	RSS, Fingerprinting, ANN	4×4×3 m	3D	-15° ∼ 15°	16 LEDs
[3]	RSS, Optimization	0.9×0.9×1.5 m	3D	0° ∼ 20°	-
[12]	AoA, Triangulation	5×1×1.5 m	2D	0° ∼ 65°	Inertial sensor
[8]	AoA, Triangulation	5×3×3 m	3D	0° ∼ 60°	Accelerometer

[1] It was judged according to whether the proposed positioning method has the pre-condition that the receiver is horizontal to the ground or is applicable even if the receiver is tilted. For the work considering the tilt, the range of the tilt is indicated.

but due to the underlying characteristics of ANN, sufficient preliminary data and complex calculations are required.

Table 1 summarizes the recent experimental studies in which a photodiode (PD) was used as a VLC receiver. To date, positioning systems have been proposed assuming specific conditions in which the height between the LED and PD is fixed or limited. The general positioning environment, where the receiver and transmitter are not facing each other in parallel, and the height is not limited, has not yet been sufficiently studied. However, in [25], a new statistical model for device orientation was established from observation results from several participants using smartphone. The authors showed that an average polar angle of 30° with a standard deviation of 9° occurs during the walking activities. Figure 1 shows a generalized VLP environment. Except for the case considering tilted receiver, the 2D positioning method can be iteratively conducted in 3D space to determine the (x, y) position of the PD, by varying the presumed height of the receiver. However, it is difficult to identify the perfect 3D position since the height, z, of the PD is only an estimated value.

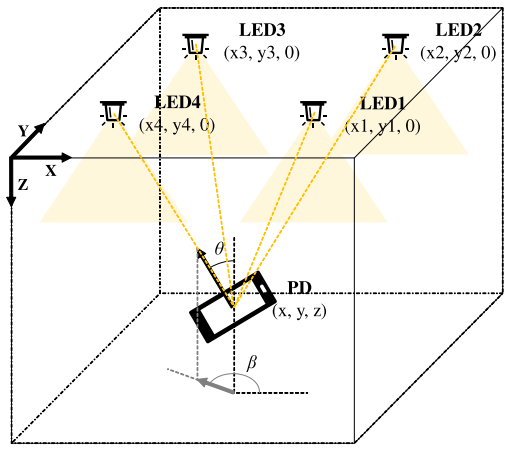

FIGURE 1. 3D VLC positioning environment.

In general, VLP algorithms use Lambertian radiation to estimate the position of the receiver using the channel gain or RSS from a specific LED. As Lambertian radiation is defined by two angles and the distance between the PD and LED, it can generally be processed in a spherical coordinate system centered on an LED [2], [8], [9]; although the formulation for a single LED location is intuitively derived, it is difficult to do the same considering all of the LED sources together. Thus, the spherical coordinate system is unsuitable for a general VLP containing multiple LEDs. To the best of our knowledge, the existing mathematical models can not represent an overall VLP system that includes multiple LEDs. The use of unified coordinate system that simultaneously reflects the locations of plural LEDs can better simplify the positioning system.

The contributions of this paper are summarized as follows:

1) We first design a VLP system model in 3D space. The tilt of the receiver, which has not been sufficiently studied yet is also considered; this system can be applied even if the receiver is not parallel to the ground. A major contribution is that the proposed model perfectly represents the entire VLP in a Cartesian coordinate system. It can cover the system with multiple LED sources using one expression within the same coordinate system. We further analyze the effect of the X, Y, and Z-axes on the RSS-based VLP and discuss the differences between the 2D and 3D methods.
2) We propose a new 3D positioning method that can be easily applied in practical indoor cases, in contrast to the 2D method with limited receiver height. The proposed method only uses the optical channel gain and receiver tilt angle information, that is, no additional

sensor assistance is required except for the device measuring the tilt. We derived the cost function of the received channel gain and distances between LEDs and an estimated position. Unlike other approaches, this approach can simplify the computations for multiple LEDs into a single expression. To justify our method, we compare several 2D and 3D positioning methods through numerical simulation.

3) Finally, we experimentally validate the performance of the proposed system. We implemented receiver and transmitter modules controlled by FPGAs, which contain digital logic designs with signal processing units. The 3D positioning results are verified by experiments in an indoor environment.

The rest of this paper is organized as follows. In section II, we describe the basic optical model, including noise models, for the VLC system. We then propose a mathematical model realizing new 3D VLP system. In addition, we examine the differences in position estimation among the X, Y, and Z-axes using the proposed model. In section III, we show the comparative results of the proposed method and those of the other existing techniques. In section IV, we discuss the practical experiments conducted using VLP and its numerical results. Finally, we present the conclusions in section V.

II. MATHEMATICAL MODEL

A. SYSTEM MODEL COMPONENTS

1) OPTICAL MODEL

In a VLC indoor positioning system, a light source (LED) is considered to be the known reference point, and the RSS method, which uses the DC gain of the optical signal at the PD, is generally applied. The LED signals are treated as Lambertian sources owing to their large beam divergence in indoor environments. Therefore, in a line-of-sight (LOS) condition, the wireless channel DC gain, H, follows the Lambertian radiation as follows [1], [2], [6], [8], [24], [26]:

$$H = \frac{(m+1)A}{2\pi d^2}\cos^m\phi\cos^n\psi\ T_s(\psi)g(\psi)\mathrm{rect}(\frac{\psi}{FOV}) \quad (1)$$

where A is the physical area of the light detector, d is the distance between the LED and PD, and ϕ and ψ are the radiation and incident angles with respect to the transmitter and receiver, respectively. $m = \frac{-\ln 2}{\ln(\cos(\phi_{1/2}))}$ and $n = \frac{-\ln 2}{\ln(\cos(\psi_{1/2}))}$, where $\phi_{1/2}$ and $\psi_{1/2}$ are the half angles of the transmitter and receiver, respectively; $T_s(\psi)$ is the optical gain of the filter and $g(\psi)$ is the concentrator gain, and the rectangular function $\mathrm{rect}(x) = 1$ for $|x| \le 1$, else, $\mathrm{rect}(x) = 0$. If the field-of-view (FOV) of the receiver is sufficiently large such that $0 \le \psi \le FOV$ is always satisfied, $\mathrm{rect}(x)$ is always equal to unity in (1). For simplicity, several studies have ignored the effects of the filter and concentrator, and have replaced them with constant values [3], [8], [9], [24].

In this work, the wireless channel gain in (1) is further simplified as follows:

$$H = K'\cos^{m'}\phi\cos^{n'}\psi\cdot d^p \quad (2)$$

Using (2), the distance, d, can be expressed using H, ϕ, and ψ as follows:

$$d = (K'\cos^{m'}\phi\cos^{n'}\psi/H)^{1/p} \quad (3)$$

2) SYSTEM NOISE MODEL

Most VLC systems operate in a variety of infrared and visible background light environments. Although received background illumination is first removed by optical filtering, shot noise is added from the remained background and signal sources [1]. In contrast, when the ambient light is sufficiently low, the dominant noise source can be thermal noise, which is also independent and Gaussian [1]. Hence, we typically model the system noise as an independent Gaussian noise with the total variance of the shot and thermal noise, as follows:

$$\sigma^2_{total} = \sigma^2_{shot} + \sigma^2_{thermal} \quad (4)$$

The shot noise originates from the fluctuations in the photodiode due to the incident optical powers of the ambient light sources. The shot noise variance is expressed as follows [1]:

$$\sigma^2_{shot} = 2q\gamma P_r B + 2qI_{bg}I_2B \quad (5)$$

where q is the electronic charge, γ is the responsivity of the PD, P_r is the received optical power, I_{bg} is the background current, I_2 is the noise bandwidth factor, and B is the equivalent noise bandwidth.

Thermal noise is due to the fluctuations in the photodiode from the temperature changes caused by the stochastic behavior of electrons. Its variance is expressed as follows [1]:

$$\sigma^2_{thermal} = \frac{8\pi kT_k}{G_0}\eta AI_2B^2 + \frac{16\pi^2k\Gamma T_k}{g_m}\eta^2A^2I_3B^2 \quad (6)$$

where k is Boltzmann's constant, T_k is the absolute temperature, G_0 is the open loop voltage gain, Γ is the channel noise factor, η is the fixed capacitance of the PD, g_m is the transconductance, and I_2 and I_3 are the noise bandwidth factors.

In section III, we verify the proposed system and compare it with various methods through simulation using (4)-(6).

B. POSITIONING SYSTEM REPRESENTATION IN 3D SPACE

In this subsection, we propose a mathematical model that is generally applicable to a 3D VLP system. In section II-B.1, to reduce the Lambertian radiation parameter, the incident angle (ψ) is replaced by the radiation and tilted angles of the receiver. In section II-B.2, an expression described by the spherical coordinate system, which is difficult to contain multiple LEDs, is converted to a Cartesian coordinate system. Finally, in section II-B.3, on the assumption that a PD exists at an arbitrary position, we determine the ideal channel gain based on the proposed VLP system.

1) REPLACEMENT OF THE INCIDENT ANGLE (ψ) WITH OTHER PARAMETERS

To simplify the system, the incident angle of the receiver is replaced by the radiation and tilt angles of the receiver.

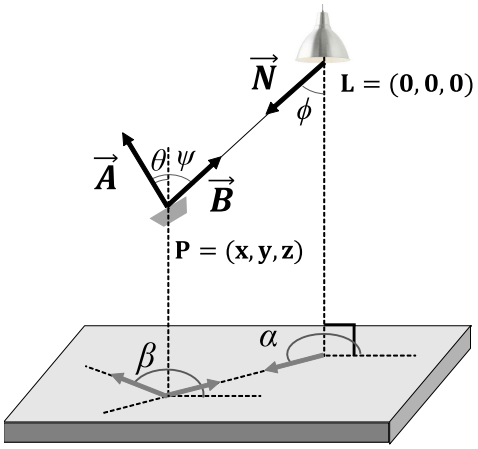

FIGURE 2. System representation in 3D space.

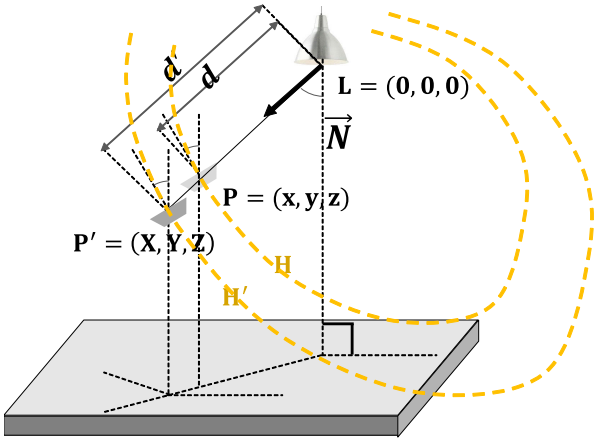

FIGURE 3. Ideal channel gain at arbitrary coordinates.

In Fig. 2, we assume that $\boldsymbol{A}$ is the normal vector of the receiver tilt and $\boldsymbol{B}$ is the unit vector of the receiver aimed at the transmitter. $\boldsymbol{A}$ and $\boldsymbol{B}$ are then expressed as follows:

$$\boldsymbol{A} = (\sin\theta\cos\beta, \sin\theta\sin\beta, -\cos\theta) \tag{7}$$

$$\boldsymbol{B} = (-\sin\phi\cos\alpha, -\sin\phi\sin\alpha, -\cos\phi) \tag{8}$$

where α is the horizontal angle at which the transmitter points toward to the receiver, and θ and β are the vertical and horizontal tilt angles of the receiver, respectively. The incident angle, ψ, is expressed by the inner product of the two vectors as follows:

$$\begin{aligned}\cos\psi &= \frac{\boldsymbol{A}\cdot\boldsymbol{B}}{|\boldsymbol{A}|\,|\boldsymbol{B}|} \\ &= -\sin\theta\cos\beta\sin\phi\cos\alpha - \sin\theta\sin\beta\sin\phi\sin\alpha \\ &\quad + \cos\theta\cos\phi \\ &= \cos\theta\cos\phi - \sin\theta\sin\phi(\cos\beta\cos\alpha + \sin\beta\sin\alpha) \\ &= \cos\theta\cos\phi - \sin\theta\sin\phi\cos(\beta-\alpha) \qquad (9) \\ \therefore \psi &= \arccos(\cos\theta\cos\phi - \sin\theta\sin\phi\cos(\beta-\alpha)) \qquad (10)\end{aligned}$$

Substituting (10) in (2), the equation for the channel gain, H, is expanded as follows:

$$\begin{aligned}H &= K'\cos^{m'}\phi\cos^{n'}\psi\cdot d^{p} \\ &= K'\cos^{m'}\phi\,(\cos\theta\cos\phi - \sin\theta\sin\phi\cos(\beta-\alpha))^{n'}\cdot d^{p}\end{aligned} \tag{11}$$

2) PARAMETER REPRESENTATION IN THE CARTESIAN COORDINATE SYSTEM

To estimate the receiver position, it is more suitable to develop a representation that can share the same location coordinates from all relevant LEDs, instead of using a specific spherical coordinate system for each LED. Therefore, it is preferable to deduce a system model with Cartesian coordinates rather than spherical coordinates. To transform a spherical coordinate system into a Cartesian one, the model representation is changed as follows.

First, we assume that the LED and receiver are located at $(0, 0, 0)$ and (x, y, z), respectively, and the unit direction vector is $\boldsymbol{N}$, as shown in Fig. 2. The coordinate, $\boldsymbol{P}$, and vector, $\boldsymbol{N}$, are expressed as follows:

$$\boldsymbol{P}(x, y, z) = d \times \boldsymbol{N} \tag{12}$$

$$\boldsymbol{N} = (\sin\phi\cos\alpha, \sin\phi\sin\alpha, \cos\phi) \tag{13}$$

Finally, using (11)-(13), the position of the receiver in the Cartesian coordinate system is calculated as follows:

$$\begin{cases} x = (K'/H)^{-1/p}\cos^{-m'/p}\phi \\ (\cos\theta\cos\phi - \sin\theta\sin\phi\cos(\beta-\alpha))^{-n'/p}(\sin\phi\cos\alpha) \\ y = (K'/H)^{-1/p}\cos^{-m'/p}\phi \\ (\cos\theta\cos\phi - \sin\theta\sin\phi\cos(\beta-\alpha))^{-n'/p}(\sin\phi\sin\alpha) \\ z = (K'/H)^{-1/p}\cos^{-m'/p}\phi \\ (\cos\theta\cos\phi - \sin\theta\sin\phi\cos(\beta-\alpha))^{-n'/p}(\cos\phi) \end{cases} \tag{14}$$

Furthermore, the horizontal and vertical angles in spherical coordinates are defined using x, y, and z as follows:

$$\cos\phi = \frac{z}{\sqrt{x^2+y^2+z^2}} \tag{15}$$

$$\sin\phi = \frac{\sqrt{x^2+y^2}}{\sqrt{x^2+y^2+z^2}} \tag{16}$$

$$\cos\alpha = \frac{x}{\sqrt{x^2+y^2}} \tag{17}$$

$$\sin\alpha = \frac{y}{\sqrt{x^2+y^2}} \tag{18}$$

3) CHANNEL GAIN ASSUMPTION

In section II-C, we present a cost function using the ratio of the distance to estimate the position of the receiver, with four LED sources, and select the position, where the cost function value is a minimum. For this purpose, the value of the ideal channel gain at any coordinate should be defined and compared with the actual received channel gain.

As shown in Fig. 3, let the reference point be located at $\boldsymbol{L} = (0, 0, 0)$. Here, we attempt to calculate the ideal

channel gain at any position, $\boldsymbol{P}' = (X, Y, Z)$. Specifically, $\boldsymbol{N}$ is the unit direction vector from $\boldsymbol{L}$ to $\boldsymbol{P}'$, where d' is the distance between $\boldsymbol{L}$ and $\boldsymbol{P}'$, and H' is the ideal channel gain value to be determined. By considering the actual measured channel gain, H, and ideal value, H', the traces of the possible positions with the same gain, according to the radiation angle, are depicted by the yellow dotted lines in Fig. 3. From L, the distance, d', is defined as follows:

$$d' = \sqrt{X^2 + Y^2 + Z^2} \tag{19}$$

By substituting (15)-(19) into (11), H' can be represented in terms of ϕ, θ, α, and β as follows:

$$\begin{aligned} H' &= K' \cos^{m'}\phi \ \cos^{n'}\psi \ d'^{p} \\ &= K' \cos^{m'}\phi \ (\cos\theta\cos\phi - \sin\theta\sin\phi\cos(\beta-\alpha))^{n'} d'^{p} \\ &= K' \cos^{m'}\phi \ (\cos\theta\cos\phi - \sin\theta\sin\phi \\ &\quad \times \ (\cos\beta\cos\alpha + \sin\beta\sin\alpha))^{n'} d'^{p} \\ &= K' \left(\frac{Z}{\sqrt{X^2+Y^2+Z^2}}\right)^{m'} \\ &\quad \times \left[\cos\theta\frac{Z}{\sqrt{X^2+Y^2+Z^2}} - \sin\theta\frac{\sqrt{X^2+Y^2}}{\sqrt{X^2+Y^2+Z^2}}\right. \\ &\quad \left. \times \left(\cos\beta\frac{X}{\sqrt{X^2+Y^2}} + \sin\beta\frac{Y}{\sqrt{X^2+Y^2}}\right)\right]^{n'} \\ &\quad \times \left(\sqrt{X^2+Y^2+Z^2}\right)^{p} \\ &= K' Z^{m'} \ (\cos\theta Z - \sin\theta\cos\beta X - \sin\theta\sin\beta Y)^{n'} \\ &\quad \times \left(X^2+Y^2+Z^2\right)^{(p-m'-n')/2} \end{aligned} \tag{20}$$

To accurately estimate the position of the receiver, the distance between the LED and estimated position should be equal to the distance calculated by the received channel gain for all of the LEDs. When considering practical cases, where various noise sources are present, the sum of the differences between these two distances for each LED must be small. In the proposed method, the cost function is designed using the ratio of the distance at the estimated position and calculated distance using the gain. We thereby calculated the cost function using H and H' for each of the four LEDs.

Previously, the position of the LED was assumed to be (0, 0, 0). However, when multiple LEDs are present in different positions, it is necessary to redefine the coordinates for each LED. As shown in Fig. 4, assuming that P_i is the receiver position, from the viewpoint of L_i, P_i can be expressed as follows:

$$P_i = (X_i, Y_i, Z_i) = (X - x_i, Y - y_i, Z - z_i) \tag{21}$$

Subsequently, the ideal channel gain for the i-th LED can be obtained using (20) and (21).

$$\begin{aligned} H_i' &= K' \cos^{m'}\phi_i \ \cos^{n'}\psi_i \ d_i'^{p} \\ &= K' Z_i^{m'} \ (\cos\theta Z_i - \sin\theta\cos\beta X_i - \sin\theta\sin\beta Y_i)^{n'} \\ &\quad \times \left(X_i^2 + Y_i^2 + Z_i^2\right)^{(p-m'-n')/2} \\ &= K'(Z - z_i)^{m'} \ (\cos\theta(Z - z_i) - \sin\theta\cos\beta(X - x_i) \\ &\quad \times \ -\sin\theta\sin\beta(Y - y_i))^{n'} \\ &\quad \times \left((X - x_i)^2 + (Y - y_i)^2 + (Z - z_i)^2\right)^{(p-m'-n')/2} \end{aligned} \tag{22}$$

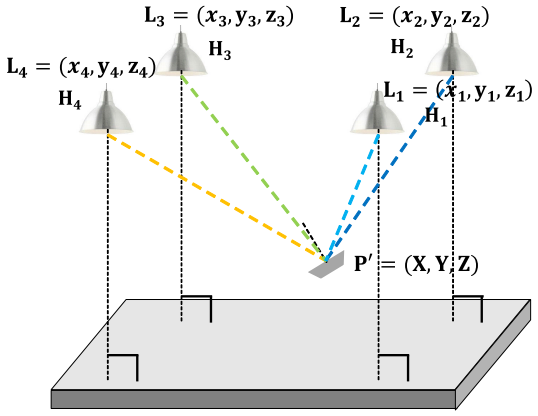

FIGURE 4. Definition of P_i for the four reference points.

Here, K', n', m', and p can be regarded as constants of the optical channel model as mentioned in section II-A.1. θ and β are predefined values that are measured, so that their trigonometric function values can be treated as constant values. Therefore, the ideal gain H_i' is represented only by the values of X, Y, and Z. Moreover, the definition can be applied to various positioning problems by adapting the gain value.

C. PROPOSED COST FUNCTION DEFINED BY THE DISTANCE RATIO

In this section, we derive the cost function used to recognize the receiver position using the ideal channel gain equation. Before deriving the cost function, we demonstrated that the estimated position of the receiver is more accurate when the difference between the actual and calculated distances from the received channel gain decreases. Therefore, we derived a new cost function that represents the ratio of the calculated distance to the actual distance, using the equation of the mathematical model shown above. In (3), the distance, d, which chiefly affects the position estimation, is defined as the product of the $1/p$-th power of the channel gain. The cost function for one LED at any point P' can then be expressed as follows.

$$Cost_i(\boldsymbol{P}') = \left(\frac{d_i' - d_i}{d_i}\right)^2 = \left(\frac{\sqrt[p]{H_i'}}{\sqrt[p]{H_i}} - 1\right)^2 \tag{23}$$

For multiple LEDs, it is necessary to determine which i-th LED signal is significant. We can herein employ the function: $D_i(P') = \text{rect}(\phi/\phi_{1/2})\text{rect}(\psi/\psi_{1/2})$ to determine whether to include consideration for the i-th LED in the entire cost function. The entire cost function for the proposed system

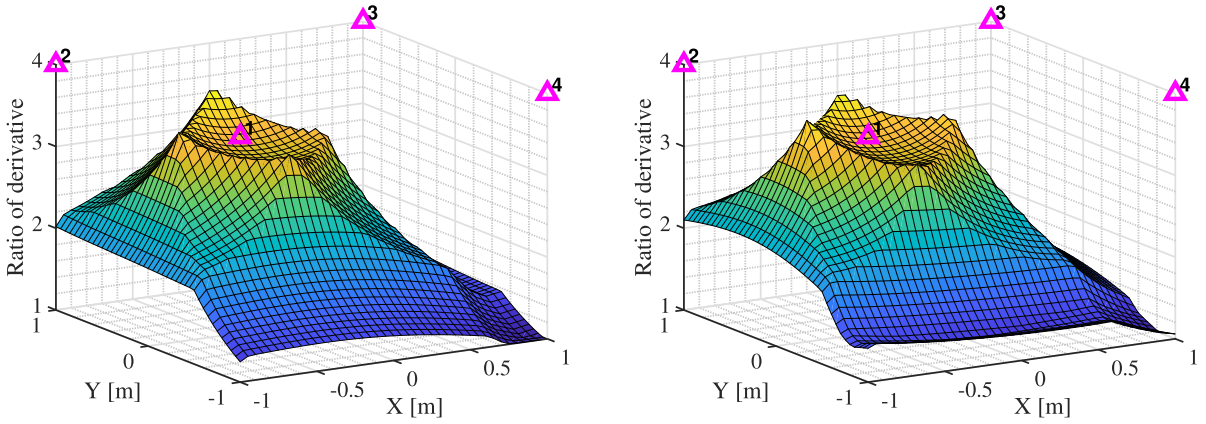

(a) Ratio of the partial derivatives of X and Z $\left(\left|\frac{\partial H}{\partial X}\right| / \left|\frac{\partial H}{\partial Z}\right|\right)$

(b) Ratio of the partial derivatives of Y and Z $\left(\left|\frac{\partial H}{\partial Y}\right| / \left|\frac{\partial H}{\partial Z}\right|\right)$

FIGURE 5. Ratio of the partial derivatives with respect to the $X-Z$ and $Y-Z$ axes.

model is then defined as follows:

$$Cost(\boldsymbol{P}') = \sum_{i=1}^{4} Cost_i(\boldsymbol{P}')\, D_i(P') = \sum_{i=1}^{4} \left(\frac{\sqrt[p]{H_i'}}{\sqrt[p]{H_i}} - 1 \right)^2 D_i(P') \tag{24}$$

D. EFFECT OF THE Z-AXIS ON POSITION ESTIMATION

The ideal channel gain, H', at any position can be obtained using (20). In this equation, the partial differentiation of the X, Y, and Z-axes can be derived as in (25)–(27).

Subsequently, we can eliminate the common term, replace $(-p + m' + n')$ with q, and substitute (9) and (19) to obtain the ratio of the partial derivatives as follows:

$$\begin{aligned} &\frac{\partial H}{\partial X} : \frac{\partial H}{\partial Y} : \frac{\partial H}{\partial Z} \\ &= -\sin\theta\cos\beta \cdot n' d'^{2} - q \cdot cos\psi \cdot X \\ &\quad : -\sin\theta\sin\beta \cdot n' d'^{2} - q \cdot cos\psi \cdot Y \\ &\quad : \frac{m'}{Z} \cdot cos\psi \cdot d'^{2} + \cos\theta \cdot n' d'^{2} - q \cdot cos\psi \cdot Z \end{aligned} \tag{28}$$

Figure 5 shows the ratio of the partial derivatives with respect to the Z axis and each X and Y axis, in a positioning environment using four LEDs and a PD. The four LEDs are placed at $(-1$ m, -1 m), $(-1$ m, 1 m), (1 m, 1 m), and (1 m, -1 m), the tilt of the PD is set to $\theta = 20°$ and $\beta = -60°$, with a height of 2 m. The ratio of the partial differential values is calculated by summing the values of the four LEDs using (28). As shown in Fig. 5, in all regions surrounded by the four LEDs where positioning generally works, the partial derivatives with respect to the X and Y axes are at least 1-4 times greater than the partial derivatives with respect to the Z-axis. Hence, the value of the partial derivative with respect to the Z-axis is always less than those of the other axes.

This further implies that the change in gain with respect to the change in the Z-axis is less than those with respect to the changes in the X or Y axes. Moreover, this indicates that when the received gain changes, the change in the estimated value of the Z-axis is less than those of the other axes. In this work, as mentioned previously, we consider an RSS-based positioning method. In RSS systems, the position of the PD is estimated by calculating the distance from the LED,

$$\begin{aligned} \frac{\partial H}{\partial X} &= |\, K' Z^{m'} (\cos\theta Z - \sin\theta\cos\beta X - \sin\theta\sin\beta Y)^{n'-1} \left(X^2+Y^2+Z^2\right)^{\frac{p-m'-n'}{2}-1} \\ &\quad \times \left[n' (-\sin\theta\cos\beta) \left(X^2+Y^2+Z^2\right) + (p-m'-n') X (\cos\theta Z - \sin\theta\cos\beta X - \sin\theta\sin\beta Y) \right] \end{aligned} \tag{25}$$

$$\begin{aligned} \frac{\partial H}{\partial Y} &= K' Z^{m'} (\cos\theta Z - \sin\theta\cos\beta X - \sin\theta\sin\beta Y)^{n'-1} \left(X^2+Y^2+Z^2\right)^{\frac{p-m'-n'}{2}-1} \\ &\quad \times \left[n' (-\sin\theta\sin\beta) \left(X^2+Y^2+Z^2\right) + (p-m'-n') Y (\cos\theta Z - \sin\theta\cos\beta X - \sin\theta\sin\beta Y) \right] \end{aligned} \tag{26}$$

$$\begin{aligned} \frac{\partial H}{\partial Z} &= K' Z^{m'} (\cos\theta Z - \sin\theta\cos\beta X - \sin\theta\sin\beta Y)^{n'-1} \left(X^2+Y^2+Z^2\right)^{\frac{p-m'-n'}{2}-1} \\ &\quad \times \left[\frac{m'}{Z} (\cos\theta Z - \sin\theta\cos\beta X - \sin\theta\sin\beta Y) \left(X^2+Y^2+Z^2\right) \right. \\ &\quad \left. + n' \cos\theta \left(X^2+Y^2+Z^2\right) + (p-m'-n') Z (\cos\theta Z - \sin\theta\cos\beta X - \sin\theta\sin\beta Y) \right] \end{aligned} \tag{27}$$

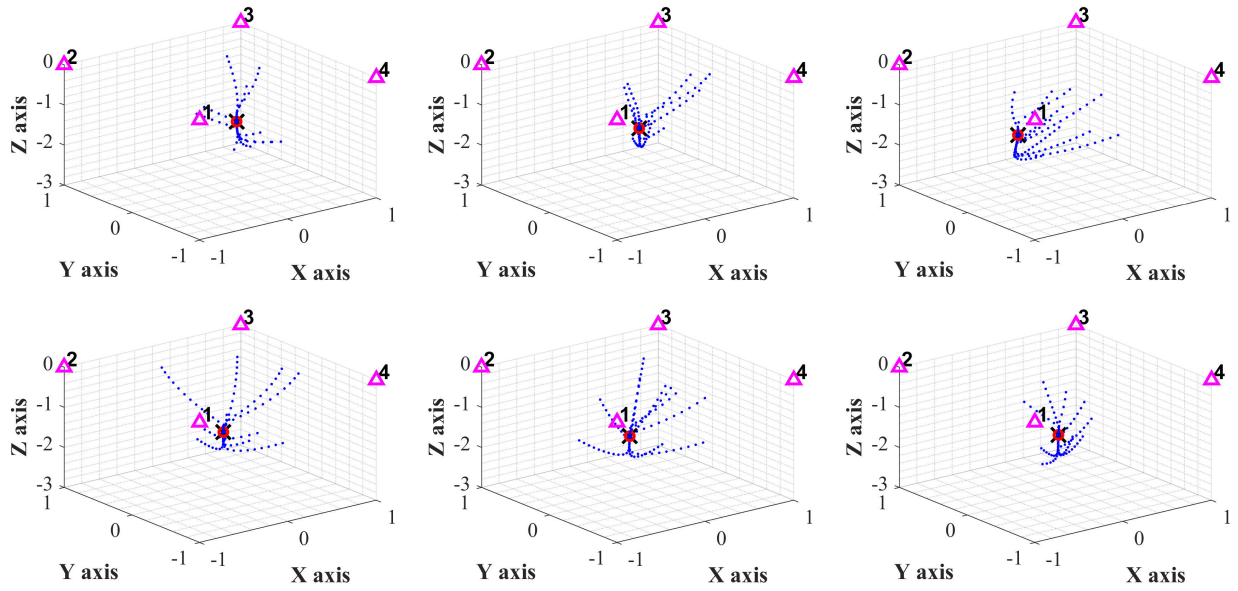

FIGURE 6. Simulation results of the position estimation with 10 random choices for the initial position and gradient search.

corresponding to the received gain. As various noise sources distort the received gain, it varies from its ideal value, causing displacement in the estimated X, Y, and Z, i.e., an error occurs. However, the obtained error for the Z-axis is smaller than those of the X and Y axes, as implied by the results of the partial derivatives. Given that the 2D positioning, which permits an incorrect Z value, can only consider the X and Y-axes values with a sufficient change, a considerable error can occur, even if there is a small change in the received gain. Conversely, as the 3D positioning additionally considers the Z-axis value with a small change, the comprehensive position error is compensated and is smaller than that of the 2D method, as demonstrated by the relevant results in section III-B.

III. SIMULATION

A. POSITION ESTIMATION RESULTS USING GRADIENT-BASED SEARCH

In the previous section, we formulated an RSS positioning system and its cost function, which can estimate the optimal receiver position in a full 3D domain. In this section, we verify the performance of the proposed cost function through a randomized simulation. The simulation environment was configured as follows: Four LEDs were located at (−1 m, −1 m, 0 m), (−1 m, 1 m, 0 m), (1 m, 1 m, 0 m), and (1 m, −1 m, 0 m), facing the floor directly. The receiver was tilted at arbitrary vertical and horizontal angles, θ and β, respectively. The receiver position was set to arbitrary values within an acceptable range, and each channel gain, H_1, H_2, H_3, and H_4, was set accordingly. In the simulation of each test, 10 random initial positions were selected, and the final estimated positions that minimized the cost function were determined for each of the 10 initial positions. We employed a gradient method to determine the point corresponding to the least cost function value. The corresponding simulation results, including the initial and refined positions, are depicted in Fig. 6. For each simulation, the determined position of the receiver is indicated by black X. In the search process for each position, the movement with the estimated coordinates is indicated by blue dots, whereas the coordinates of the final positions of each trial are indicated by red circles. As shown in Fig. 6, even if the initial positions are randomly selected, all of the final determined positions converge to the receiver's position. We can see that the gradient search can also be used to directly find the solution.

B. COMPARISON WITH OTHER METHODS

In this section, we compare the performance of the proposed method with other existing PD-based VLP methods. The simulation setup satisfies the following conditions. Four LEDs were placed at (−0.25 m, −0.5 m, 0 m), (0.5 m, −0.25 m, 0 m), (0.25 m, 0.5 m, 0 m), and (−0.5 m, 0.25 m, 0 m). For each trial, the receiver location to be estimated was randomly selected within a 0.5 m × 0.5 m area. As mentioned in section II-A.2, to model the system noise, white Gaussian noise with a 20-dB SNR was added for ideal channel gain values. Additive Gaussian noise yields a random error during the transmission and reception of the VLC system, so adding noise with the same SNR ensures that the signal quality of the multiplexing process is the same for all methods. The random error can be better reduced depending on the type of multiplexing process.

For comparison, we selected 2D and 3D VLP methods that were verified experimentally. We have implemented other positioning algorithms directly in MATLAB by referring to their suggesting paper. The authors of [19], [20] and [21]

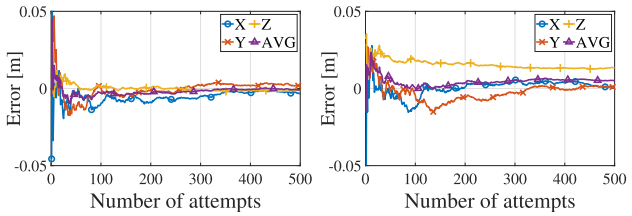

(a) Error for the proposed method (b) Error for [19]

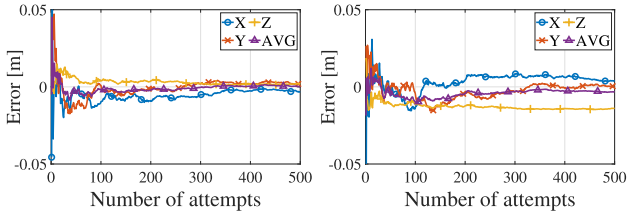

(c) Error for [3] (d) Error for [20], [21]

FIGURE 7. Errors in the X, Y, and Z axes for each method.

applied a trilateration method for a 2D plane. They derived several squared equations using the positions of the LEDs and the receiver, and combining those equations to derive the plane coordinates of the receiver. To apply these methods to 3D space, we decided on a solution with the smaller $X - Y$ error within the valid range of the Z-axis height. Furthermore, these methods are not applicable when the receiver is tilted. Cai *et al.* [3] proposed a 3D positioning algorithm based on the global optimization technique. To implement the algorithm of [3], we have selected a position that minimizes the proposed fitness function, which consists of the square sum of the difference between the measured channel gain and the ideal channel gain derived by the currently chosen position of the receiver for each LED. Also, [3] method compensates the result for the receiver tilt. In addition, consideration has been given to recently proposed methods using ANN architecture [22], [23]. Since, these methods require sufficient pre-measured data and have limitation in their application to unlearned areas, the comparison with the proposed method is not appropriate.

Several comparisons were made with existing methods according to various criteria. The errors in the X, Y, and Z-axes in Cartesian coordinates, were first separately accumulated for each method (Fig. 7). The 3D Euclidean errors for the cumulated and averaged axis error were subsequently, compared (Fig. 8a). Finally, the expected values of the 3D Euclidean errors for each trial were compared (Fig. 8b). In the first comparative simulations, the PD tilt was not applied to have a fair comparison with the other methods, which do not consider the tilt. The comparative results are discussed below.

For each method, the respective position errors along the X, Y, and Z-axes were accumulated according to the number of trials, as shown in Fig. 7. The 3D positioning methods, including our work and [3], exhibited near-zero errors along the Z-axis. The error bound was not large compared to those of the other 2D methods. This is because it is not possible for

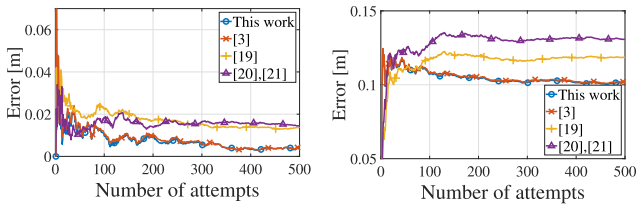

(a) 3D errors obtained from the averaged axis error (b) Averaged 3D errors for all the trials

FIGURE 8. Comparison of the 3D euclidean errors for each method.

the 2D methods to correctly identify the Z-axis coordinate. Apparently, this is a disadvantage of the 2D method, which calculates only two axes and estimates the Z-axis, compared to the 3D method, which collectively calculates all three axes.

In Figs. 8a and 8b, we employ two metrics for comparison, namely, the 3D error of the cumulated and averaged axis errors, and the expected 3D error for each trial, respectively. In Fig. Fig. 8a, when the number of trials increase, the errors of the 2D methods do not converge to zero; the error has a certain bias compared to that of the 3D methods in which the error converges to zero. As shown in Fig. 8b, the expected positioning errors are relatively high in the 2D methods, indicating that the positioning error for each trial is greater than those in the 3D methods.

The performances of the proposed method and [3] were similar. Further simulations were conducted for the two methods. Given that [3] also corrects the tilt of the receiver, the tilt was randomly varied with the position of the receiver for each trial. The number of trials was greater than that in the previous simulation, and more error results were accumulated. As shown in Fig. 9, the proposed method had less 3D errors, compared to [3]. The improvement in positioning becomes obvious at low SNR (=15 dB in Fig. 9a). The simulation shows that the accuracy of the proposed method is improved by 2-7% compared with the method of [3].

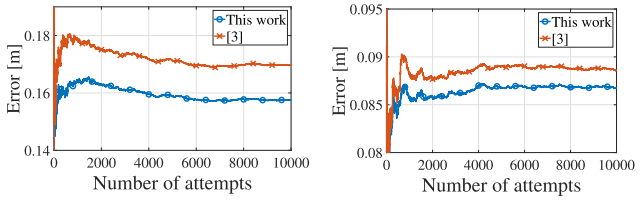

(a) SNR = 15 [dB] (b) SNR = 20 [dB]

FIGURE 9. Comparison of the 3D errors of the proposed method and [3].

IV. EXPERIMENT

A. EXPERIMENTAL SCENARIO

In this work, the 3D positioning was conducted within a 2.5 m × 2.5 m × 3 m space in a laboratory. The PD module was setup so that it could be inclined at any angle. Four LEDs were installed at the corners of an 88 cm × 88 cm square.

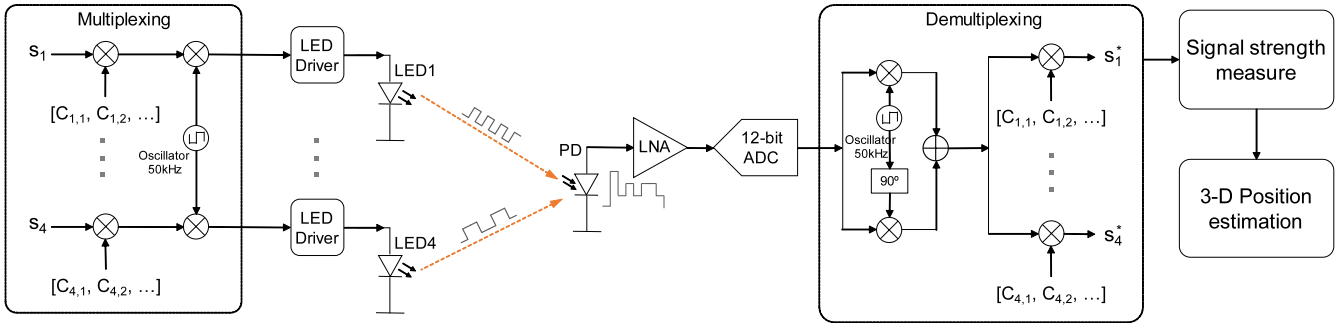

FIGURE 10. Overall signal processing flow diagram.

The experimental procedure is as follows. We first calculated the value of the Lambertian parameters in (3) using one LED and one PD by varying the distance, incident angle, and radiation angle. We subsequently used four LEDs and one PD to measure the channel gain for each LED, while adjusting the position and tilt angle of the PD. Finally, we estimated the position of the receiver using the received channel gain and tilt of the PD.

B. EXPERIMENTAL SETUP

We implemented LED and PD modules that could be separately controlled by two FPGAs. Four white (6000-7000 K) LEDs (SJ-3W-CW) and a silicon PIN photodiode (SD 100-14-21-021) were used for the VLC driver and receiver designs. In the transmitting part, the LED and current switch were configured to operate through the enabling signal from the FPGA. In the receiving part, the PD and amplifier sensed the optical signal. The FPGA obtained the received information through a 12-bit A/D converter operating at 12 MHz.

Figure 10 shows the overall signal processing procedure, from the light source to the receiver. In this work, the Hadamard matrix was employed to multiplex the multi-channel optical signals and demultiplex the combined signal into the independent channel components. In our previous work [27], we demonstrated that this approach greatly reduces random errors in low-cost VLC systems. First, in the FPGA of the transmitting part, each row of a 4^{th} order Hadamard matrix was mixed with a 50-kHz oscillator and used to transmit signals. The transmitted electrical signals cause the respective LED to emit through an LED driver. Then the PD receives the sum of the four optical signals reduced from each LED. The signal received from the PD is sent to the receiver FPGA through a 12-bit ADC. In the receiving part of the FPGA, in-phase/quadrature (IQ) demodulation is performed on the received signal. Each row of the Hadamard matrix is multiplied to extract the signal component (RSS) for each LED. The channel gain for each LED is then obtained, and 3D positioning can be performed.

Figure 11 displays the LED and PD modules used in the experiment. Figure 11a shows the configuration of the transmission part that includes four PCBs for driving the LEDs and a main PCB for controlling each LED. This main PCB is equipped with an FPGA module that sends the Hadamard-encoded signal to each LED PCB as the enabling signal. It also supplies power to each LED PCB, which includes an LED driver. Thus, the LED can be appropriately driven through the enabling signal generated by the main PCB. The four LED boards are arranged on the flat plate at equal intervals of 0.88 m. Figure 11b shows the configuration of the receiving part. The signal passing through the PD and low-noise amplifier (LNA) are delivered to the FPGA module through the 12-bit ADC. The receiver PCB is attached to the holder and can be easily tilted and fixed at the designated angle. For accurate and precise demultiplexing, the receiver and transmitter are connected with a wire for synchronization.

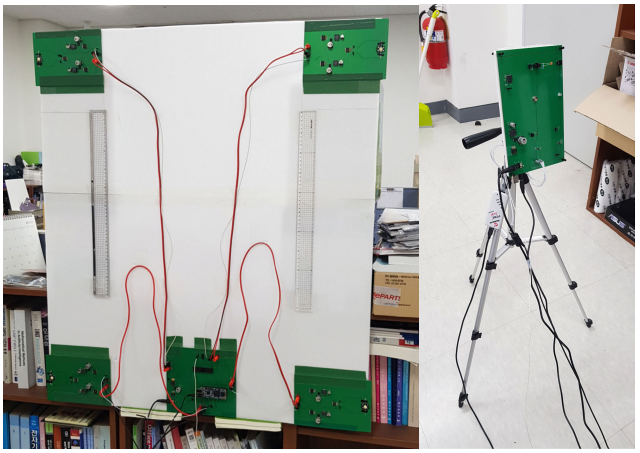

(a) Transmitter (4 LEDs, FPGA module) **(b)** Receiver (PD, FPGA module)

FIGURE 11. Hardware configuration for the experiment.

C. PARAMETER FITTING FOR THE LAMBERTIAN RADIATION PATTERN

Before 3D positioning, it is necessary to experimentally determine the value of each parameter of the Lambertian radiation given by (2) using a characterized link between the LED and

PD. For the measurement, the PD and LED were arranged side-by-side, and their angles were set to 0, 15, 30, and 45°, and 0, 15, 30, 45, and 60°, respectively. The distance between the PD and LED was also varied to 1.8, 2.25, 2.7, 3.15, and 3.6 m. Figure 12 presents a graph that compares the measured gain to the estimated pattern function with respect to the incident angle (PD) and radiation angle (LED). Five graphs for each distance are overlapped simultaneously in the figure. Reflecting the characteristics of all elements in the transmitter and receiver module, including the amplifier and LED driver, Lambertian parameters were experimentally determined as shown in Table 2.

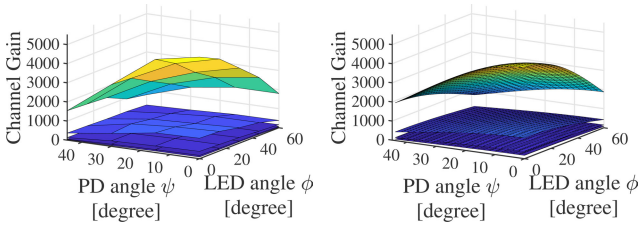

(a) Measured channel gain value at specific points with respect to ϕ and ψ

(b) Estimated channel gain value with respect to ϕ and ψ

FIGURE 12. Results of the measurements and estimated channel gain functions.

TABLE 2. Parameters of the 3-D positioning system.

Parameter	Value
Space Size (L × W × H) / m	2.5 × 2.5 × 3
LED Position (x, y, z) / m	LED1 (-0.44, -0.44, 0) LED2 (0.44, -0.44, 0) LED3 (0.44, 0.44, 0) LED4 (-0.44, 0.44, 0)
The FOV of the LEDs / deg	125 ± 5
The FOV of the PD / deg	82
The optical filter gain ($T_s(\psi)$)	1.0
The optical concentrator gain ($G(\psi)$)	1.0
Determined Lambertian parameters (K', m', n', p)	(3252, 2.684, 1.350, -3.636)
Height of the receiver (z) / m	1.5, 2.0, 2.5
Plane position of the receiver (x, y) / m	(-0.25, -0.25) to (0.25, 0.25), 0.25 interval for each axis
Receiver tilt (θ, β) / deg	(0, 0), (15, 0), (15, 15) (30, 0), (30, 15), (30, 30)

D. 3D POSITION ESTIMATION USING THE PROPOSED COST FUNCTION

The 3D positioning algorithm was practically applied to an indoor environment, which included four LEDs and one PD. We selected the minimum value of the proposed cost function as the final estimated position of the receiver. The four LED coordinates were (−0.44 m, −0.44 m, 0 m), (0.44 m, −0.44 m, 0 m), (0.44 m, 0.44 m, 0 m), and (−0.44 m, 0.44 m, 0 m). The test positions of the receiver were varied to 1.5, 2.0, and 2.5 m (Z-axis), based on the origin. A total of nine testing positions were utilized at 0.25 m intervals, within horizontal coordinates corresponding to (−0.25 m, −0.25 m) and (0.25 m, 0.25 m). The testing was repeated, while changing the vertical and horizontal tilts of the receiver to (0°, 0°), (15°, 0°), (15°, 15°), (30°, 0°), (30°, 15°), and (30°, 30°). The parameters of the 3-D positioning are summarized in Table 2. During the test, using the tilt of the receiver, cases where the incidence angle was greater than the FOV ($\psi > \psi_{1/2}$) were excluded.

In summary, the 3D positioning was performed and analyzed for 101 test cases, with three distance values, nine horizontal positions, and six pairs of tilted angles. The overall positioning results are shown in Fig. 13, and the results are plotted in 3D space and 2D cross-section planes.

The average 3D error of the experiment results was 7.95 cm. However, 70% of the errors had an average value within 5.5 cm. A histogram of the 3D errors is depicted in Fig. 14. Main causes of the position error have been summarized as follows. Firstly, there were shot and thermal noise effects observed at PD. Secondly, measurement errors occurred. For example, when setting the tilt and measurement position of the receiver, the ideal and actual values may have differed slightly. In addition, other noise components have occurred from the internal noise of the transmitting/receiving board including the noise of the ADC, and noise from the power and ground. Furthermore, the LED light could have been reflected by walls, the ceiling, the desk, and any other obstacles within the room, causing multipath effects.

Performance analysis results according to each criterion are summarized in Tables 3 and 4. There were almost no differences with a standard deviation of less than 0.52 cm in the performances with regard to the tilt. However, the results in the center portion, where the signal intensities became relatively equal, were better than those in the edge regions.

TABLE 3. Position estimation results based on several criteria.

Criteria	Parameter Value		
	Average Error [cm]		
Tilted Angle	0°, 0°	15°, 0°	15°, 15°
	8.080	8.218	7.437
	30°, 0°	30°, 15°	30°, 30°
	8.086	6.981	8.509
X [cm]	-25	0	25
	7.713	8.237	7.910
Y [cm]	-25	0	25
	8.298	6.662	8.773
Z (distance) [cm]	150	200	250
	6.003	8.539	8.878

TABLE 4. Position estimation results based on the horizontal position.

Average Error [cm]		X [cm]		
		-25	0	25
Y [cm]	25	5.331	8.784	10.312
	0	5.573	5.912	6.278
	-25	8.106	12.818	9.485

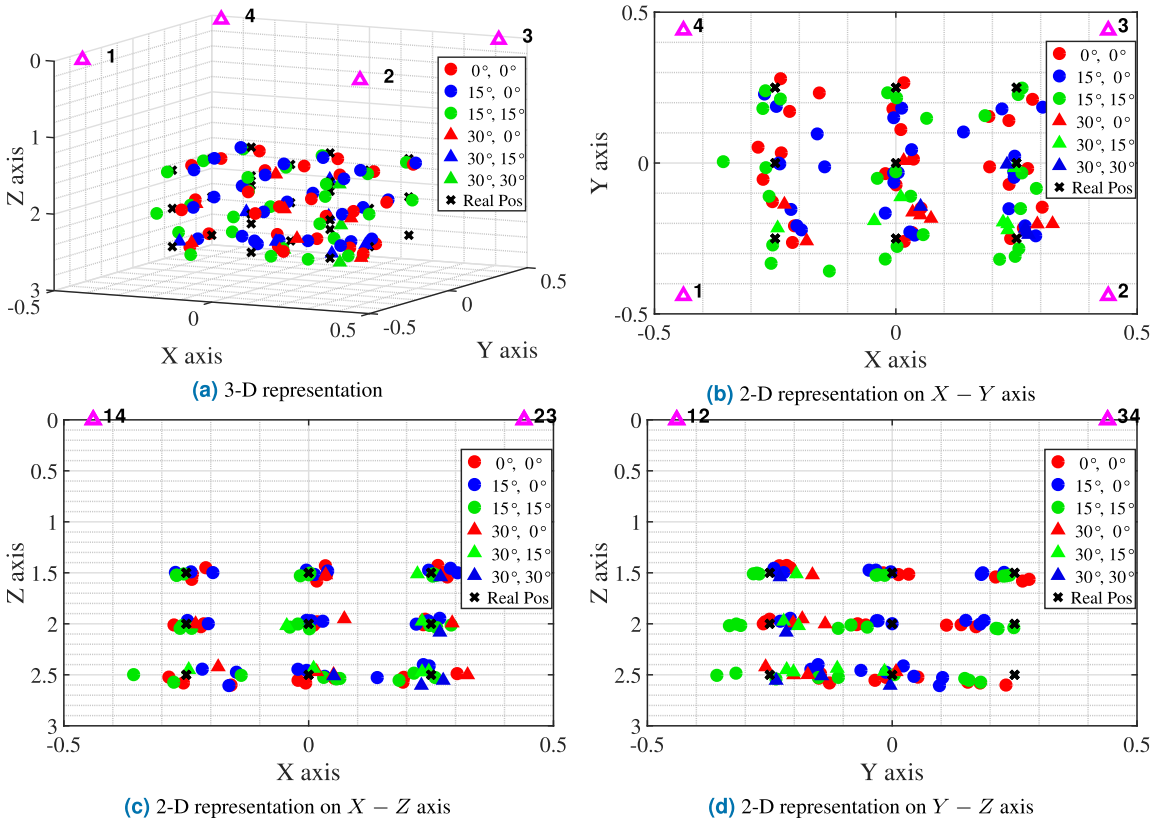

(a) 3-D representation

(b) 2-D representation on $X - Y$ axis

(c) 2-D representation on $X - Z$ axis

(d) 2-D representation on $Y - Z$ axis

FIGURE 13. Position estimation results in 3D space.

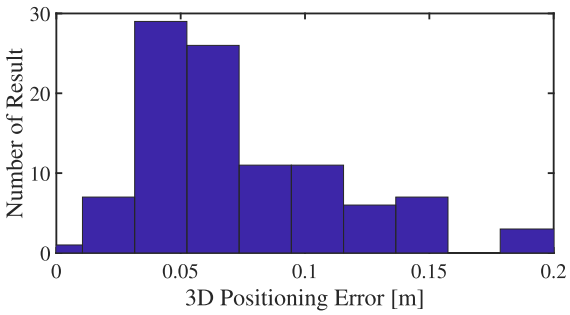

FIGURE 14. Histogram of the 3D positioning error.

The closer the distance, the better the observed accuracy. Additionally, as discussed in section II-D, the Z error is much less than the X and Y errors for 3D positioning. This is obviously seen in Figs. 13b-d. In Fig 13b, the results are spread wider on the X and Y planes, whereas the results in Figs 13c and 13d are gathered about the Z-axis.

V. CONCLUSION

In this paper, we presented a new VLC-based positioning method in 3D space that considers the tilt of the receiver, which has not been sufficiently studied previously. The proposed method does not require additional devices, other than the receiver tilt information. The simulation results indicated that our work contains the lowest errors compared to other recent 2D and 3D positioning methods. A system model applicable to general VLC positioning systems was newly formulated, that considers the effect of the height and receiver tilt; the proposed model conforms to a system using multiple LEDs, based on a Cartesian coordinate system. Additionally, we analyzed the effect of the X, Y, and Z-axes on the positioning, and presented the differences between the 2D and 3D positioning methods. Practical positioning experiments were conducted in an indoor environment, and the determined average error of the proposed method was 7.95 cm. The results demonstrated that there were almost no differences with a standard deviation of about 0.52 cm in the performance, with respect to the receiver tilt.

REFERENCES

[1] Q. Wang and H. Luo, "Light positioning: A high-accuracy visible light indoor positioning system based on attitude identification and propagation model," *Int. J. Distrib. Sensor Netw.*, vol. 14, no. 2, pp. 1–14, Feb. 2018.

[2] M. Yasir, S.-W. Ho, and B. N. Vellambi, "Indoor position tracking using multiple optical receivers," *J. Lightw. Technol.*, vol. 34, no. 4, pp. 1166–1176, Feb. 15, 2016.

[3] Y. Cai, W. Guan, Y. Wu, C. Xie, Y. Chen, and L. Fang, "Indoor high precision three-dimensional positioning system based on visible light communication using particle swarm optimization," *IEEE Photon. J.*, vol. 9, no. 6, pp. 1–20, Dec. 2017.

[4] D. Karunatilaka, F. Zafar, V. Kalavally, and R. Parthiban, "LED based indoor visible light communications: State of the art," *IEEE Commun. Surveys Tuts.*, vol. 17, no. 3, pp. 1649–1678, Aug. 2015.

[5] A. Sevincer, A. Bhattarai, M. Bilgi, M. Yuksel, and N. Pala, "LIGHTNETs: Smart LIGHTing and mobile optical wireless NETworks—A survey," *IEEE Commun. Surveys Tuts.*, vol. 15, no. 4, pp. 1620–1641, 4th Quart., 2013.
[6] H.-S. Kim, D.-R. Kim, S.-H. Yang, Y.-H. Son, and S.-K. Han, "An indoor visible light communication positioning system using a RF carrier allocation technique," *J. Lightw. Technol.*, vol. 31, no. 1, pp. 134–144, Jan. 1, 2013.
[7] S. H. Yang, H. S. Kim, Y. H. Son, and S. K. Han, "Three-dimensional visible light indoor localization using AOA and RSS with multiple optical receivers," *J. Lightw. Technol.*, vol. 32, no. 14, pp. 2480–2485, Jul. 15, 2014.
[8] M. Yasir, S.-W. Ho, and B. N. Vellambi, "Indoor positioning system using visible light and accelerometer," *J. Lightw. Technol.*, vol. 32, no. 19, pp. 3306–3316, Oct. 1, 2014.
[9] L. Li, P. Hu, C. Peng, G. Shen, and F. Zhao, "Epsilon: A visible light based positioning system," in *Proc. 11th USENIX Symp. Netw. Syst. Design Implement. (NSDI)*, vol. 14, 2014, pp. 331–343.
[10] Z. Li, A. Yang, H. Lv, L. Feng, and W. Song, "Fusion of visible light indoor positioning and inertial navigation based on particle filter," *IEEE Photon. J.*, vol. 9, no. 5, pp. 1–13, Oct. 2017.
[11] J. Vongkulbhisal, B. Chantaramolee, Y. Zhao, and W. S. Mohammed, "A fingerprinting-based indoor localization system using intensity modulation of light emitting diodes," *Microw. Opt. Technol. Lett.*, vol. 54, no. 5, pp. 1218–1227, 2012.
[12] C. Sertthin, E. Tsuji, M. Nakagawa, S. Kuwano, and K. Watanabe, "A switching estimated receiver position scheme for visible light based indoor positioning system," in *Proc. 4th Int. Symp. Wireless Pervasive Comput. (ISWPC)*, Feb. 2009, pp. 1–5.
[13] B. Xie, K. Chen, G. Tan, M. Lu, Y. Liu, and J. Wu, "LIPS: A light intensity–based positioning system for indoor environments," *ACM Trans. Sensor Netw.*, vol. 12, Nov. 2016, Art. no. 28.
[14] Q. Zou, W. Xia, Y. Zhu, J. Zhang, B. Huang, F. Yan, and L. Shen, "A VLC and IMU integration indoor positioning algorithm with weighted unscented Kalman filter," in *Proc. 3rd IEEE Int. Conf. Comput. Commun. (ICCC)*, Chengdu, China, Dec. 2017, pp. 887–891.
[15] L. Wang, C. Guo, P. Luo, and Q. Li, "Indoor visible light localization algorithm based on received signal strength ratio with multi-directional LED array," in *Proc. IEEE Int. Conf. Commun. Workshops (ICC Workshops)*, Paris, France, May 2017, pp. 138–143.
[16] J.-Y. Wang, J.-B. Wang, B. Zhu, M. Lin, Y. Wu, Y. Wang, and M. Chen, "Improvement of BER performance by tilting receiver plane for indoor visible light communications with input-dependent noise," in *Proc. IEEE Int. Conf. Commun. (ICC)*, Paris, France, May 2017, pp. 1–6.
[17] B. Zhu, J. Cheng, J. Yan, J. Wang, and Y. Wang, "VLC positioning using cameras with unknown tilting angles," in *Proc. IEEE Global Commun. Conf. (GLOBECOM)*, Singapore, Dec. 2017, pp. 1–6.
[18] B. Zhu, J. Cheng, Y. Wang, J. Yan, and J. Wang, "Three-dimensional VLC positioning based on angle difference of arrival with arbitrary tilting angle of receiver," *IEEE J. Sel. Areas Commun.*, vol. 36, no. 1, pp. 8–22, Jan. 2018.
[19] Y. C. See, N. M. Noor, and Y. M. C. Tan, "Investigation of indoor positioning system using visible light communication," in *Proc. IEEE Region Conf. (TENCON)*, Singapore, Nov. 2016, pp. 186–189.
[20] B. Lin, X. Tang, Z. Ghassemlooy, C. Lin, and Y. Li, "Experimental demonstration of an indoor VLC positioning system based on OFDMA," *IEEE Photon. J.*, vol. 9, no. 2, Apr. 2017, Art. no. 7902209.
[21] S. Yamaguchi, V. V. Mai, T. C. Thang, and A. T. Pham, "Design and performance evaluation of VLC indoor positioning system using optical orthogonal codes," in *Proc. IEEE 5th Int. Conf. Commun. Electron. (ICCE)*, Danang, Vietnam, Jul./Aug. 2014, pp. 54–59.
[22] J. He, C.-W. Hsu, Q. Zhou, M. Tang, S. Fu, D. Liu, L. Deng, and G.-K. Chang, "Demonstration of high precision 3D indoor positioning system based on two-layer ANN machine learning technique," in *Proc. Opt. Fiber Commun. Conf. (OFC)*, 2019, pp. 1–3.
[23] I. Alonso-González, D. Sánchez-Rodríguez, C. Ley-Bosch, and M. A. Quintana-Suárez, "Discrete indoor three-dimensional localization system based on neural networks using visible light communication," *Sensors*, vol. 18, no. 4, p. 1040, 2018.
[24] H. Chen, W. Guan, S. Li, and Y. Wu, "Indoor high precision three-dimensional positioning system based on visible light communication using modified genetic algorithm," *Opt. Commun.*, vol. 413, pp. 103–120, Apr. 2018.
[25] M. D. Soltani, A. A. Purwita, Z. Zeng, H. Haas, and M. Safari, "Modeling the random orientation of mobile devices: Measurement, analysis and LiFi use case," May 2018, *arXiv:1805.07999*. [Online]. Available: https://arxiv.org/abs/1805.07999
[26] J. M. Kahn and J. R. Barry, "Wireless infrared communications," *Proc. IEEE*, vol. 85, no. 2, pp. 265–298, Feb. 1997.
[27] J. K. Park, T.-G. Woo, M. Kim, and J. T. Kim, "Hadamard matrix design for a low-cost indoor positioning system in visible light communication," *IEEE Photon. J.*, vol. 9, no. 2, Apr. 2017, Art. no. 7801710.

DUCKYONG KIM received the B.S. degree from the Department of Electrical and Computer Engineering, Sungkyunkwan University, Suwon, South Korea, in 2017, where he is currently pursuing the integrated M.S. and Ph.D. degrees. His current research interests include the sensor signal processing and embedded system design.

JONG KANG PARK (M'15) received the B.S. and M.S. degrees in electric, electronics and computer engineering and the Ph.D. degree in electric and electronics engineering from Sungkyunkwan University, South Korea, in 2001, 2003, and 2008, respectively. From 2008 to 2013, he was with Samsung Electronics, where he designed touch sensor ICs and multi-touch algorithms. He is currently a Research Professor with the School of Electronic and Electrical Engineering, Sungkyunkwan University. His current research interests include the sensor signal processing, embedded system design, soft error analysis, and tolerance techniques.

JONG TAE KIM (M'86) received the B.S. degree in electronics engineering from Sungkyunkwan University, South Korea, in 1982, and the M.S. and Ph.D. degrees in electrical and computer engineering from the University of California at Irvine, Irvine, in 1987 and 1992, respectively. From 1991 to 1993, he was with Aerospace Corporation, Elsegundo, California. He was a full-time Lecturer with Chunbuk National University, South Korea, from 1993 to 1995. Since 1995, he has been with the School of Electronic and Electrical Engineering, Sungkyunkwan University, as a Professor. His research interests include sensor systems, brain-inspired computing and architecture, embedded systems, and the IoT.